



PCCP

Exciton Dynamics in Heterojunction Thin-Film Devices Based on Exciplex-Sensitized Triplet-Triplet Annihilation

Journal:	<i>Physical Chemistry Chemical Physics</i>
Manuscript ID	CP-ART-08-2018-005261.R1
Article Type:	Paper
Date Submitted by the Author:	17-Oct-2018
Complete List of Authors:	Tierce, Nathan; University of California at Riverside, Chemistry Chen, Chia-Hsun ; National Taiwan University, Institute of Photonics and Optoelectronics, Department of Electrical Engineering Chiu, Tien-Lung; Yuan Ze University, Department of Photonics Engineering Lin, Chi-Feng; National United University, 1 Lienda Road, Miaoli 36003, Republic of China, Department of Electro-Optical Engineering Bardeen, Christopher; University of California at Riverside, Chemistry LEE, JIUN-HAW; National Taiwan University, Institute of Photonics and Optoelectronics, Department of Electrical Engineering

SCHOLARONE™
Manuscripts

Exciton Dynamics in Heterojunction Thin-Film Devices Based on Exciplex-Sensitized Triplet- Triplet Annihilation

Nathan T. Tierce,^{†,1} Chia-Hsun Chen,^{†,2} Tien-Lung Chiu,³ Chi-Feng Lin,⁴

Christopher J Bardeen,^{,1} and Jiun-Haw Lee^{*,2}*

¹Department of Chemistry, University of California, Riverside, Riverside, CA 92506, United States

²Graduate Institute of Photonics and Optoelectronics and Department of Electrical Engineering, National Taiwan University, 1, Sec. 4, Roosevelt Road Taipei, Taiwan, R.O.C., 10617

³Department of Electrical Engineering, Yuan Ze University, 135 Yuan-Tung Road, Taoyuan, Taiwan, R.O.C, 32003

⁴Department of Electro-Optical Engineering, National United University, 1, Lienda Road, Miaoli, Taiwan, R.O.C., 36003

ABSTRACT: Exciton dynamics in a solid-state exciplex sensitized triplet-triplet annihilation (ESTTA) system are studied using transient photoluminescence (TrPL) measurements. The ESTTA system is a trilayer structure with 4, 4', 4''-tris(N-3-methylphenyl-N-phenyl-amino) triphenylamine (m-MTDATA) acting as the electron donor, 1-(2,5-dimethyl-4-(1-pyrenyl)phenyl)pyrene (DMPPP) as a triplet-diffusion-singlet-blocking (TDSB) layer, and 9,10-bis(2'-naphthyl) anthracene (ADN), acting as the electron acceptor and emitter. The thicknesses of the m-MTDATA and ADN layers are 30 nm, while the thickness of the DMPPP layer is varied to characterize its effect on the singlet quenching of the ADN emission. We find that electron transfer via tunneling through the DMPPP layer is the dominant quenching channel, with a characteristic length of ~ 5 nm. Doping the high photoluminescence quantum yield molecule 4,4'-bis[2-(4-(*N,N*-diphenylamino)phenyl)vinyl]biphenyl (DPAVBi) into the ADN layer enhanced the overall intensity of the ESTTA signal but did not prevent quenching by exciplex formation. The trilayer configuration (m-MTDATA/DMPPP/ADN) can effectively prevent ADN singlets from being quenched by electron transfer and exciplex formation, and a key property of the DMPPP is its tendency to not undergo electron transfer to the ADN.

1. Introduction

One strategy for generating stable blue emitting organic light emitting diodes (OLEDs) is to utilize triplet-triplet annihilation (TTA) to avoid high-energy singlet-singlet annihilation processes¹⁻⁴. In such a device, electrons and holes recombine to generate 25% singlets and 75% triplets, and the triplets then undergo TTA to create more singlets for light emission. To improve the efficiency of this process, sensitized TTA-OLED devices incorporate two materials: a low-bandgap sensitizer to generate triplets and a wide-bandgap emitter that supports the TTA process^{5, 6}. In a sensitized TTA system, the sensitizer can be pumped optically or electrically, then transfer energy to the low-energy triplet state of the emitter via triplet energy transfer (TET). Two triplet excitons then undergo TTA to generate an emitter molecule in its singlet state, which then emits fluorescence⁷⁻¹⁰. The quantum efficiency of the TTA upconversion process, defined as the number of singlet state photons divided by the number of triplets, can approach the theoretical limit of 50% in the solution phase¹¹. The mobility of molecules in liquid solution allows the TET and TTA events to be widely separated in space and prevents the high-energy singlet state of the emitter from being quenched by low-energy states of the sensitizer. In solid-state architectures, physical proximity of sensitizer and emitter increases the probability of singlet quenching (SQ) of the emitter by the low-bandgap sensitizer^{12, 13}. Suitable control of molecular aggregation of sensitizer and emitter may help improve the efficiency^{14, 15} but a bilayer structure (such as sensitizer/emitter) is preferred for solid-state STTA¹⁶. Even in a bilayer, SQ can still occur at the sensitizer/emitter interface. Increasing the emitter layer thickness can reduce SQ by increasing the average distance between the TTA event and the interface^{17, 18}. However, a thicker layer also increases the film resistance, which can degrade the performance of organic optoelectronic devices like OLEDs and organic solar cells.

Molecular exciplexes have been used as both emitters¹⁹⁻²³ and triplet sensitizers^{24, 25} in OLEDs. In previous work, we demonstrated that using a trilayer geometry could significantly improve the performance of a blue OLED device based on exciplex-sensitized triplet-triplet annihilation (ESTTA)¹⁷. In these devices, the exciplex was generated at the heterojunction interface of electron donor and acceptor materials, 4, 4', 4''-tris(N-3-methylphenyl-N-phenyl-amino) triphenylamine (m-MTDATA) and 9,10-bis(2'-naphthyl) anthracene (ADN), as shown in Fig. 1 (a). Efficient intersystem crossing in the charge-transfer exciplex results in facile TET to the ADN triplet, followed by blue emission after TTA. However, the efficiency in a bilayer was low due to SQ of the ADN singlet state, as shown in Fig. 1(b). A 40× improvement in efficiency was achieved by: (1) insertion of a triplet-diffusion and singlet blocking (TDSB) layer between sensitizer and emitter, and (2) incorporation of fluorescent dopant inside the TTA emitter, as shown in Fig. 1 (c). The detailed device performance data can be found in reference 17. For those devices, 1-(2,5-dimethyl-4-(1-pyrenyl)phenyl)pyrene (DMPPP) was used as the TDSB, as shown in Fig. 1 (d)²⁶. This molecule has a triplet energy between that of the exciplex and ADN, allowing triplets to migrate through the DMPPP layer to the ADN. But its singlet energy is higher than that of both the exciplex and ADN, so it can block singlet quenching of ADN by the exciplex. Doping the ADN layer with the high PL quantum yield emitter 4,4'-bis[2-(4-(*N,N*-diphenylamino)phenyl)vinyl]biphenyl (DPAVBi) further improved the device efficiency²⁷.

In the present paper, we seek to understand the physical origins of the improvement in the device EQE observed previously¹⁷. We are particularly interested in the relative roles of the singlet blocking versus the dopant in preventing SQ. In this paper, transient photoluminescence (TrPL) measurements of bilayer and trilayer thin films that consist of various combinations of the donor, TDSB, and emitter layers are performed to investigate the exciton dynamics. We find

that the TDSB layer makes the most important contribution to the suppression of SQ. But even for the thickest DMPPP layers, we still find evidence for ADN singlet quenching which generates a long-range m-MTDATA/ADN exciplex that extends across the TDSB layer. The fluorescent dopant is also clarified. Our results suggest that there is room for improvement in the ESTTA devices by optimizing material parameters like the TDSB energy levels and the dopant fluorescence quantum yield.

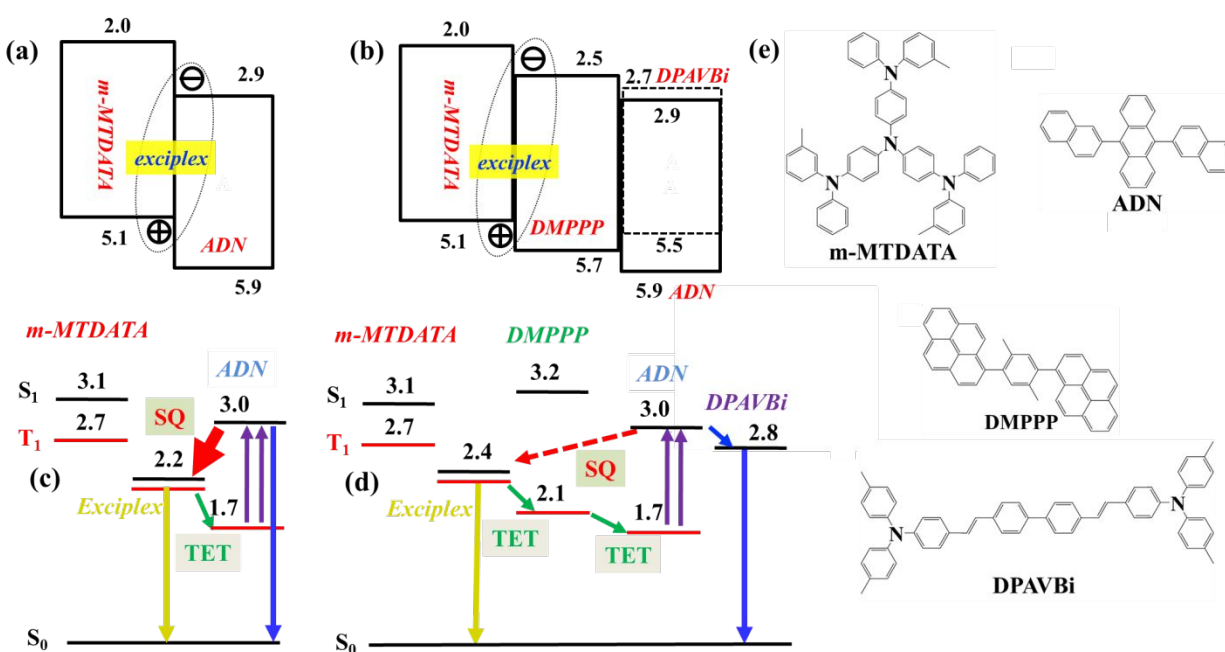


Figure 1. Device outline and energy level diagrams of ESTTA-OLED with bilayer ((a) and (c)) and TDSB+dopant ((b) and (d)) configuration, respectively, along with the molecular structures (e).

2. Experimental Section

Thin-film fabrication: Organic thin films were deposited on the glass substrate by thermal evaporator under 5×10^{-6} torr. Prior to thin-film deposition, the glass substrate was cleaned by acetone, methanol, and water for 5 min in a supersonic bath, followed by oxygen plasma

treatment (50 sccm, 30 mtorr, 18 W for 5 mins). Calibrated crystal monitors on the evaporation sources were used to obtain the thickness of each layer with a resolution to 0.1 nm and to control the dopant concentration to 0.1%. After thin-film evaporation, the samples were sent for encapsulation to a glove box that kept water and oxygen concentrations below 1 ppm. The cover glass was cleaned using the same procedure as the substrate. An ultraviolet-sensitive epoxy was applied on the periphery of the cover glass for assembly of sample and cover glass, followed by ultraviolet exposure.

TrPL measurement of organic thin film: Time-resolved measurements were performed with a 1 kHz Coherent Libra regeneratively amplified Ti:Sapphire laser system. The 800 nm fundamental pulse was directed into a frequency doubling beta barium borate crystal to produce the 400 nm excitation beam. The encapsulated sample was mounted on a translation stage and the emission was collected using front face detection with a 420 nm long pass filter. The emission was detected using a Hamamatsu C4334 Streakscope with 25 ps time resolution and 2.5 nm wavelength resolution. Typical laser powers were 10-20 microwatts, and no dependence of the early (< 100 ns) signal on laser power was observed, indicating that exciton-exciton annihilation was negligible in this time window. The TrPL decay curves shown in the following figures represent data integrated over a range of wavelengths to improve the signal-to-noise. Wavelength selected traces are provided in the Supporting Information when relevant.

3. Results and Discussions

We first characterized the photophysical behavior of thin films composed of pure m-MTDATA, DMPPP, and ADN separately. Figure 2 (a) shows the absorption spectra of the different organic thin films with 30 nm thickness. The ADN layer absorbed much more efficiently at 400 nm than the m-MTDATA and DMPPP thin-films. Figure 2 (b) shows the normalized PL spectra of the three thin films taken within 1 ns after 400 nm laser excitation. The broad emission lineshapes peak at 441, 461, and 438 nm for m-MTDATA, DMPPP, and ADN, respectively. Figure 2 (c) shows the un-normalized PL spectra, showing that under the same conditions, the ADN emission intensity was $\sim 40\times$ stronger than that of m-MTDATA and DMPPP. It is therefore safe to assume that the PL signal after 400 nm excitation will be dominated by emission from ADN singlet excitons.

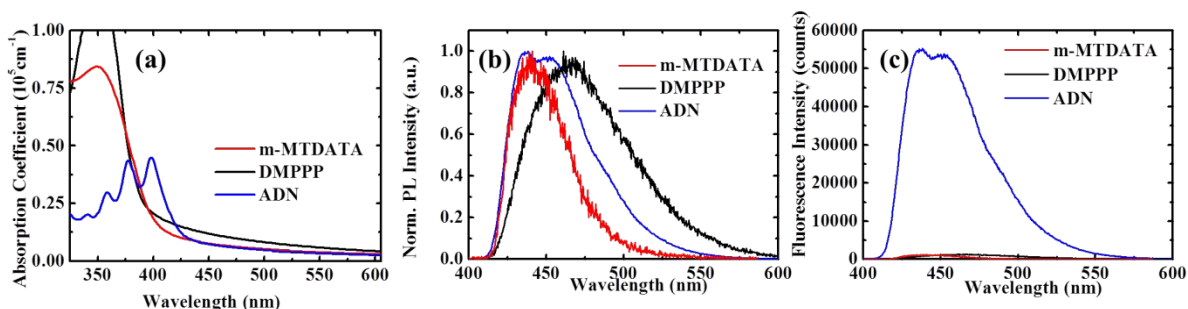


Figure 2. (a) Absorption spectra, (b) normalized PL spectra, and (c) un-normalized PL spectra of single-component m-MTDATA (red lines), DMPPP (black lines), and ADN (blue lines) thin films.

We next characterized the exciplex states in the bilayer films. Exciplex emission was observed from both m-MTDATA/DMPPP and m-MTDATA/ADN films, with peaks at 491 and 521 nm respectively, together with singlet emission from m-MTDATA, DMPPP and ADN

ranging from 438 nm to 461 nm. No exciplex emission was observed for the DMPPP/ADN bilayers (Supporting Information). Figure 3 (a) shows the PL spectra of the bilayer films m-MTDATA/DMPPP (30 nm/ 30 nm) and m-MTDATA/ADN (30 nm/30 nm), integrated over a 5 μ s window. The emission wavelength of m-MTDATA/DMPPP was shorter than m-MTDATA/ADN due to the shallower LUMO value of DMPPP (2.5 eV), compared to that of ADN (2.9 eV), as shown in Fig. 1 (d). Figure 3 (b) shows the transient photoluminescence (TrPL) measurement on the μ s timescale. For the m-MTDATA/DMPPP and m-MTDATA/ADN bilayer thin films, a fast decay from the singlet states of DMPPP and ADN is followed by slower exciplex emission decays with time constants of 0.15 and 0.21 μ s, respectively. In contrast, the ADN film PL signal completely decays within 200 ns.

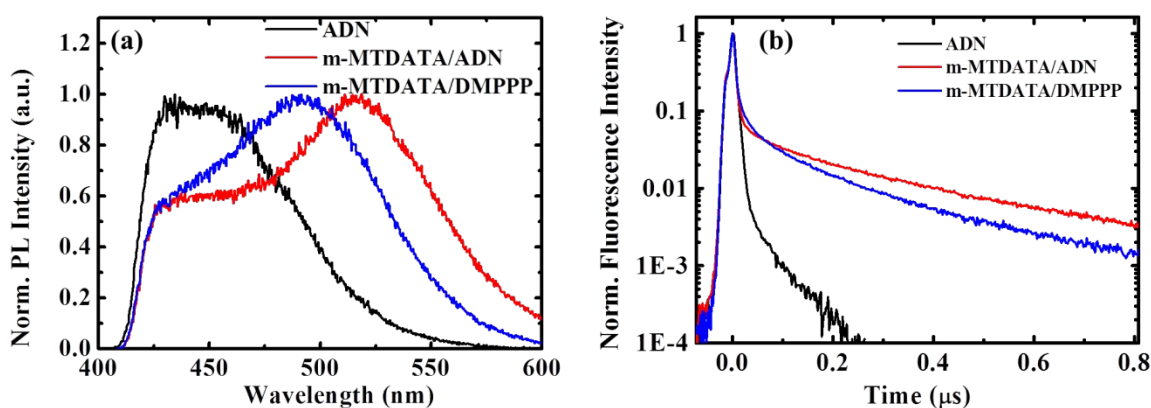


Figure 3. (a) PL spectra integrated from 0-5 microseconds, of ADN thin film (black) and bilayer films of m-MTDATA/ADN (red) and m-MTDATA/DMPPP (blue). (b) TrPL decay of ADN thin film (black) and bilayer films of m-MTDATA/ADN (red) and m-MTDATA/DMPPP (blue) integrated from 400-600 nm. The ADN decay dominates at short times (<200 ns), while the exciplex decay dominated on the microsecond scale.

To examine quenching of the ADN singlet by exciplex formation, we first examined the DMPPP/ADN interface. As shown in Fig. 4 (a), the TrPL decay of the DMPPP/ADN bilayer

was identical to ADN. Hence, we can say that DMPPP/ADN bilayer did not affect the (singlet) exciton dynamics of the ADN layer. On the other hand, for a m-MTDATA/ADN (30 nm/30 nm) bilayer film, the ADN singlet emission exhibited a reduced decay time as shown in Fig 4 (a). The ADN decay could be slowed down by inserting DMPPP between the m-MTDATA and ADN layers. In these trilayer samples, the decay time increased with increasing DMPPP thickness, as shown in Fig. 4 (b). As expected, the singlet exciton in ADN was blocked by the DMPPP layer from reaching the m-MTDATA/DMPPP exciplex due to the wider bandgap of DMPPP (3.2 eV) as compared to ADN (3.0 eV). The exciplex emission did not affect the analysis of the ADN singlet dynamics on the sub-ns timescale, as shown by single wavelength TrPL decays (Supporting Information, Figure S1).

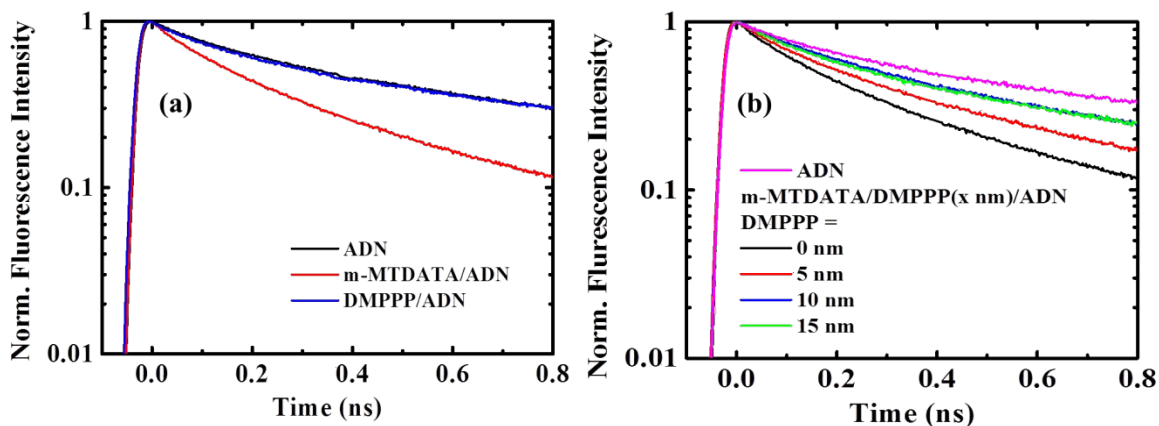


Figure 4. (a) Early time (0.0-0.8 ns) TrPL decays of monolayer ADN, and bilayers m-MTDATA/ADN, and DMPPP/ADN. (b) trilayer m-MTDATA/DMPPP/ADN with different DMPPP thickness (0, 5, 10, 15 nm), and single layer ADN thin films. TrPL decays were integrated from 400-600 nm and are dominated by the ADN contribution on this timescale.

The mechanism of ADN SQ merits some discussion. In principle, energy transfer to an exciplex state could proceed by an electron transfer process or by direct energy transfer via the

Forster or Dexter mechanism.²⁸ Due to the low oscillator strength of the exciplex ground state, most models of exciplex formation assume it occurs through electron transfer with a rate that falls off exponentially with distance.²⁹⁻³¹ If the electron transfer from the m-MTDATA to the ADN occurs by tunneling across the entire DMPPP layer, we would expect k_q to decay exponentially with TDSB layer thickness R . If, on the other hand, electron transfer at the DMPPP interface occurs, then the electron can hop through the DMPPP layer, leading to a much weaker distance dependence. These two mechanisms leading to exciplex formation are illustrated in Fig. 5. Given that we observed no quenching of the ADN fluorescence by a DMPPP layer, electron transfer from this layer is probably not competitive with the ADN singlet decay. Therefore we will concentrate on the tunneling mechanism for electron transfer and quenching.

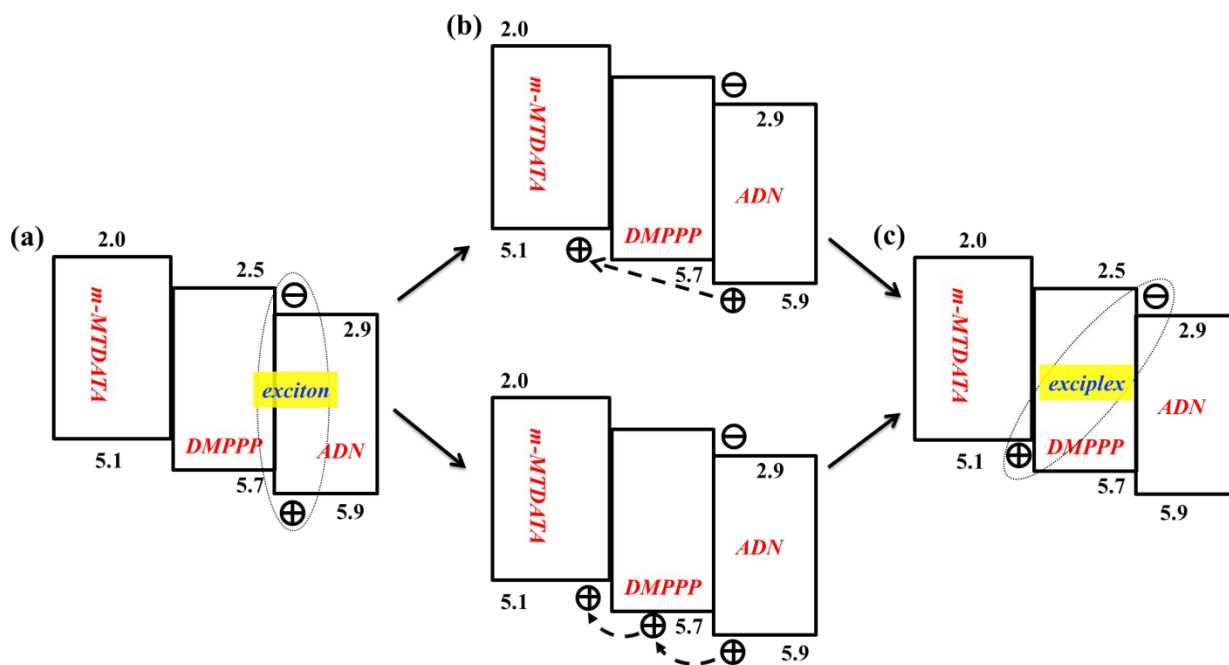


Figure 5. Schematic diagram of different pathways for ADN exciton quenching by charge transfer and exciplex formation. In the upper pathway, the hole travels from the ADN to the m-MTDATA directly through tunneling. In the bottom pathway, the hole can hop through the DMPPP layer before reaching the m-MTDATA. Both pathways lead to the formation of a long-range exciplex between m-MTDATA and ADN.

The TrPL signal of the ADN (integrated from 410-450 nm) could be fit using a biexponential decay of the form

$$TrPL(t) = [Ae^{-k_A t} + Be^{-k_B t}] e^{-k_q t} \quad (1)$$

where k_A and k_B are the intrinsic decay rates of the ADN thin film and k_q is the rate of quenching by exciplex formation. Fitting the ADN thin film data yields $A = B = 0.50 \pm 0.03$, $k_A = 5.6 \pm 0.2 \text{ ns}^{-1}$, and $k_B = 0.8 \pm 0.1 \text{ ns}^{-1}$. By keeping these parameters constant and varying k_q , we could obtain good fits to the TrPL decays in Figure 4(b). From the discussion in the preceding paragraph, we approximate the dependence of k_q on R by,

$$k_q(R) = k_q^{tun} e^{-\alpha R} \quad (2)$$

Fitting the k_q data in Fig. 6 with Equation (2) yields $k_q^{tun} = 13.3 \text{ ns}^{-1}$ and $\alpha = 0.16 \text{ nm}^{-1}$. Despite the fact that we only have four points, Equation (2) provides a reasonably good fit to the data in Fig. 6. The $\alpha = 0.16 \text{ nm}^{-1}$ value lies within the range observed for charge recombination across an organic spacer layer³² but is small compared to typical values obtained for molecular donor-bridge-acceptor complexes.^{33, 34} The DMPPP layer may aid the electron transfer by supporting superexchange contributions to the coupling between ADN and m-MTDATA layers^{35, 36}, but the exact mechanism of photoinduced charge transport across solid-state organic semiconductor layers is largely unexplored³⁷.

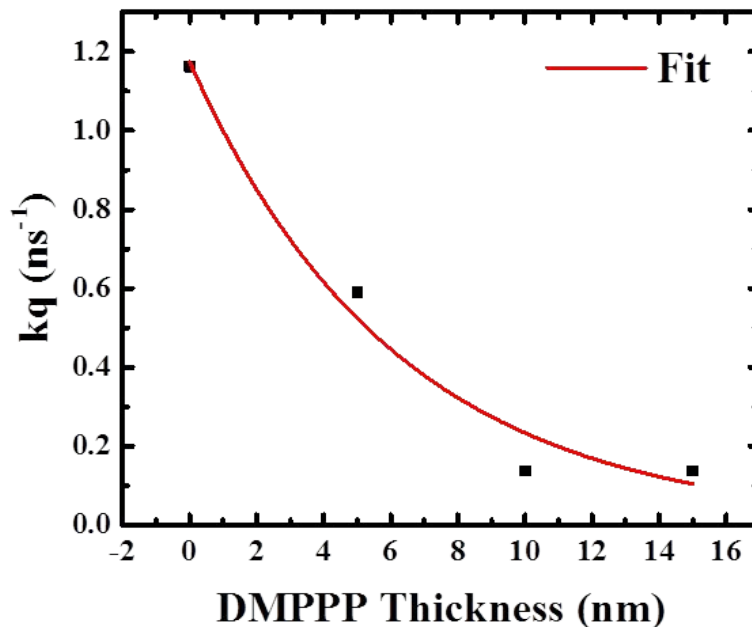


Figure 6. Plot of $k_q(R)$, where R = thickness of the DMPPP layer, along with a fit using Equation (2) in the text.

In all cases, electron transfer across the TDSB layer leads to a final state in which the hole resides in the m-MTDATA and the electron in the ADN. The presence of this exciplex state is indeed observed in the PL of the trilayer systems. Immediately after photoexcitation, the normalized PL spectra of the trilayer (m-MTDATA/DMPPP/ADN) thin films with different DMPPP thicknesses were identical, showing only the ADN fluorescence peaked at 448 nm (Fig. 7(a)). However, when measuring the PL spectra at long time-scales (1.42-2.64 μs), both blue and yellow emission peaks at 448 and 521 nm were observed as shown in Fig. 7(b). The 521 nm emission corresponds to the m-MTDATA/ADN exciplex, while the long-lived 448 nm emission can be assigned to TTA in the ADN. No sign of the m-MTDATA/DMPPP exciplex at 491 nm is observed even for the 15 nm thick DMPPP layer.

The 448 nm/521 nm peak ratio depends on the DMPPP layer thickness in a complicated way. On the one hand, a thinner TDSB layer facilitates formation of the exciplex state that sensitizes the ADN triplet and leads to the delayed fluorescence from TTA. Without an exciplex state, intersystem crossing is negligible for ADN and no delayed fluorescence is observed. On the other hand, once formed, the ADN singlet will experience more quenching for thinner DMPPP layers. These two competing effects lead to an increase in the delayed blue emission with DMPPP layer thicknesses up to 10 nm, followed by a decrease for $R = 15$ nm. The optimum thickness must be in the 10-15 nm range.

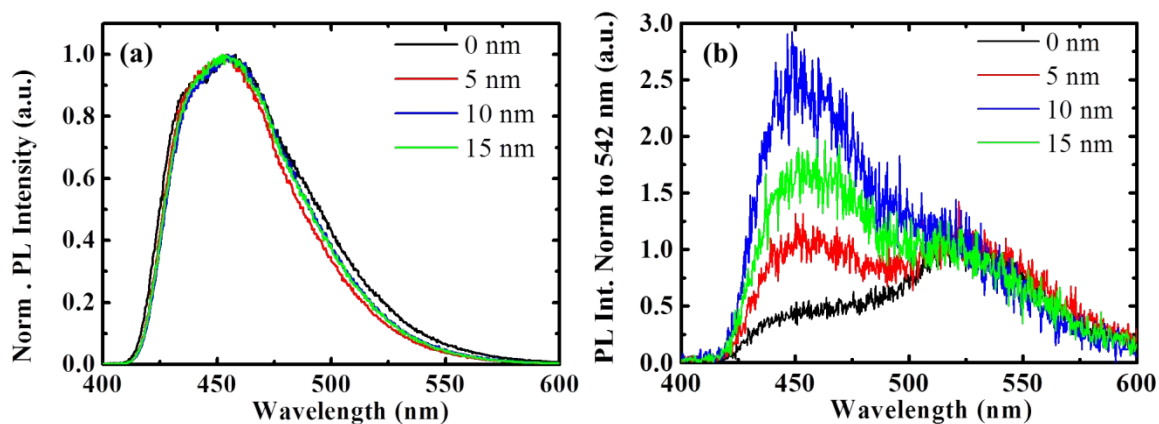


Figure 7. (a) Early (0.0-1.0 ns) and (b) late (1.4-4.6 μ s) PL spectra of ADN-DMPPP-MTDATA trilayer films with different DMPPP thicknesses. The ADN and m-MTDATA thicknesses were 30 nm. The maximum enhancement of the upconverted ADN PL is observed for a DMPPP thickness of 10 nm, as seen for OLED devices.

The absence of DMPPP quenching and exciplex emission suggests that this molecule does not transfer an electron the photoexcited ADN, despite the fact that its HOMO lies 0.2 eV above that of ADN. It is likely that kinetic factors prevent electron transfer between ADN and DMPPP from competing with the ADN singlet decay. For example, there is evidence from

solution studies that steric effects can slow or prevent exciplex formation.^{38, 39} On the other hand, electron transfer between m-MTDATA and ADN appears to be quite facile. The observation of the m-MTDATA/ADN exciplex state emission even with a relatively thick TDSB layer was surprising, given that there is no physical interface between the m-MTDATA and the ADN. Previous work has shown that it is possible to form a long-range exciplex between electron donor and acceptor materials that sandwich a spacer layer^{40, 41}. Perhaps surprisingly no emission due to the m-MTDATA/DMPPP exciplex was observed after optical excitation, in contrast to the electrically pumped OLED devices. This difference probably originates from the fact that in electrically pumped devices, the relative mobilities of injected electrons and holes determine where recombination and exciplex formation occur. From our previous work¹⁷, it appears that charges accumulate at the m-MTDATA/DMPPP interface, as shown in Fig. 1 (b). For optical excitation of the ADN at 400 nm, there is no voltage bias to drive charges across the TDSB layer and only the long-range m-MTDATA/ADN exciplex is formed.

Rather than using the TDSB layer to prevent SQ, a complementary strategy is to dope the emitter layer with a lower energy emissive molecule as an exciton trap. DPAVBi is a highly efficient fluorescent molecule that can be readily incorporated into the ADN layer. We hypothesized that it might trap the ADN singlets produced by TTA before they could diffuse to the DMPPP/ADN interface and undergo charge transfer to form the exciplex. Fig. 8(a) shows the TrPL decay of DPAVBi doped into ADN with a 10% in volume ratio. This doping level was found to be optimal for the OLED devices studied previously. Energy transfer from ADN to DPAVBi was very efficient, and in the 10% film most of the emission came from DPAVBi. When this doped layer was combined with a m-MTDATA layer, the DPAVBi lifetime decreased significantly, as shown in Fig. 8(a). All the decays were parameterized as biexponentials as

defined in Equation (1), and by fitting the bilayer data in the inset of Fig. 8(a) we could extract a value $k_q = 1.0 \pm 0.1 \text{ ns}^{-1}$. This value is very similar to that of neat ADN (1.2 ns^{-1}), suggesting that singlet excitons can still diffuse through the emitter layer. The idea that the DPAVBi component could prevent singlet exciton quenching is not supported by the data. The main benefit of adding this dopant appears to be its higher fluorescence quantum yield as compared to ADN.

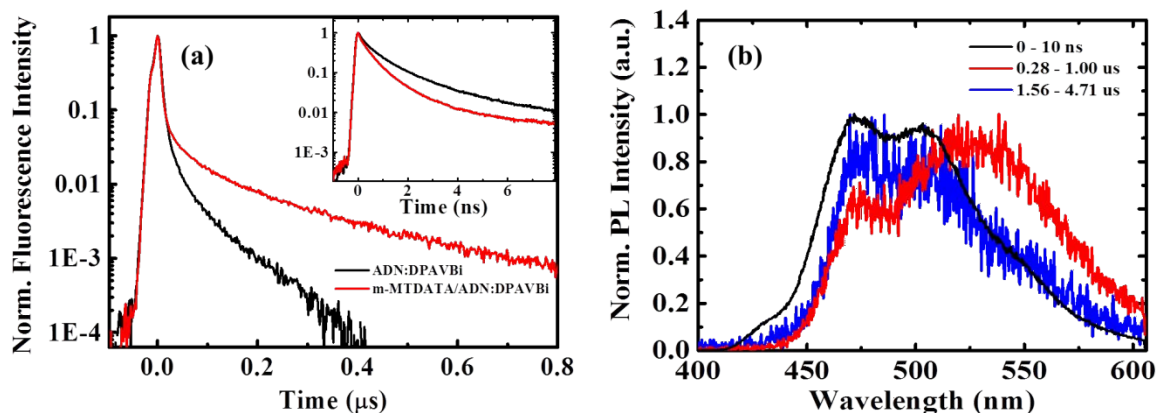


Figure 8. (a) *inset*: TrPL intensity within 8 ns window of DPAVBi doped into ADN and ADN m-MTDATA bilayer with 10% in volume ratio. TrPL decays were integrated from 400-600 nm and reflect DPAVBi and exciplex components at short and long times, respectively. (b) PL spectra of doped bilayer at early, medium and late time windows.

The DPAVBi SQ would be expected to be accompanied by m-MTDATA-ADN exciplex formation. Without the m-MTDATA layer, the ADN:DPAVBi mixed film TrPL signal completely decayed within 400 ns, as shown in Fig. 8(a). With the m-MTDATA, the bilayer film exhibited a long-lived decay, similar to that of the m-MTDATA/ADN exciplex. The presence of the long-time decay suggests that some long-lived exciplex is created. The spectral evolution of the TrPL shown in Fig. 8(b). The initial period of the TrPL signal is dominated by the DPAVBi spectrum after energy transfer from the ADN. This fluorescence shows a strong

exciplex contribution at intermediate times (0.3-1.0 μs) after photoexcitation. These exciplex states can then sensitize triplets in the ADN, and on even longer timescales (1.5-4.7 μs) the PL spectrum shifts back to the DPAVBi emission (peaks at 472 and 502 nm) due to sensitized TTA in the ADN layer, followed by rapid energy transfer to the DPAVBi.

4. Summary

The results reported here clarify how a TDSB layer composed of DMPPP could act to boost the efficiency of blue emitting OLEDs, as observed in our previous work.¹⁷ We have demonstrated that this enhancement results from the ability of the DMPPP layer to effectively block ADN singlets from being quenched by electron transfer and exciplex formation. In addition to the energetic requirements for a TDSB layer (a triplet energy gap that lies between that of the sensitizer and emitter, and a singlet energy gap greater than both), we find that it must also avoid exciplex formation and charge transfer from the emitter. DMPPP is a molecule that fulfills these requirements with respect to m-MTDATA and ADN. Adding a fluorescent dopant molecule to the ADN layer enhances the TTA signal, mainly due to its greater fluorescence quantum yield as opposed to inhibiting exciton diffusion. Finally, we should point out that the m-MTDATA/DMPPP/ADN trilayer system is not fully optimized, and there is room to improve output by finding materials that suppress SQ even more. The results in this paper suggest that TDSB energy level engineering can benefit the development of optoelectronic devices based on triplet exciton dynamics.

SUPPORTING INFORMATION

Electronic Supporting Information available: Additional PL spectra and decays, along with fits.

AUTHOR INFORMATION

Corresponding Authors

Email: jiunhawlee@ntu.edu.tw

Email: christopher.bardeen@ucr.edu

† NT and CHC contributed equally to this work.

ACKNOWLEDGMENT

This work was supported by the Ministry of Science and Technology (MOST), R.O.C under Grants No. MOST 102-2221-E-002-182-MY3, 104-2221-E-002 -156 -MY3, 105-2221-E-002 -130- MY3, 105-2221-E-239-024, 105-3113-E-155-001, 104-3113-E-155-001, 103-3113-E-155-001, 103-2221-E-155-028-MY3, 107-2221-E-002-156-MY3, 106-2923-E-002-004-MY3, and 105-2221-E-155-239-024, and by the National Science Foundation grant DMR-1508099 (CJB).

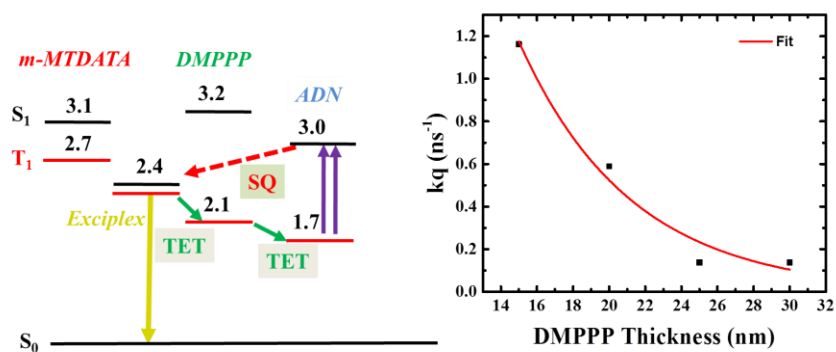
REFERENCES

1. C.-J. Chiang, A. Kimyonok, M. K. Etherington, G. C. Griffiths, V. Jankus, F. Turksoy and A. P. Monkman, *Adv. Funct. Mater.*, 2013, **23**, 739–746.
2. N. A. Kukhta, T. Matulaitis, D. Volyniuk, K. Ivaniuk, P. Turyk, P. Stakhira, J. V. Grazulevicius and A. P. Monkman, *J. Phys. Chem. Lett.*, 2017, **8**, 6199–6205.
3. T. Masuda, Y. Nakano, Y. Takahashi, H. Ito, K. Okinaka, E. Kambe, Y. Kawamura and H. Kuma, *J. Soc. Inf. Disp.*, 2018, **26**, 146–152.
4. Y. Takita, K. Takeda, N. Hashimoto, S. Nomura, T. Suzuki, H. Nakashima, S. U. S. Seo and S. Yamazaki, *J. Soc. Inf. Disp.*, 2018, **26**, 55–63.
5. X. Qiao, P. Yuan, D. Ma, T. Ahamad and S. M. Alshehri, *Org. Electron.*, 2017, **46**, 1–6.
6. C. Xiang, C. Peng, Y. Chen and F. So, *Small*, 2015, **11**, 5439–5443.
7. M. K. Manna, S. Shokri, G. P. Wiederrecht, D. J. Gosztola and A. J. L. Ayitou, *Chem. Commun.*, 2018, **54**, 5809–5818.
8. T. N. Singh-Rachford and F. N. Castellano, *Coord. Chem. Rev.*, 2010, **254**, 2560–2573.
9. N. Yanai and N. Kimizuka, *Chem. Commun.*, 2016, **52**, 5354–5370.
10. N. Yanai and N. Kimizuka, *Acc. Chem. Res.*, 2017, **50**, 2487–2495.
11. F. Deng, J. Blumhoff and F. N. Castellano, *J. Phys. Chem. A*, 2013, **117**, 4412–4419.
12. V. Gray, K. Moth-Poulsen, B. Albinsson and M. Abrahamsson, *Coord. Chem. Rev.*, 2018, **362**, 54–71.
13. R. Karpicz, S. Puzinas, V. Gulbinas, A. Vakhnin, A. Kadashchuk and B. P. Rand, *Chem. Phys.*, 2014, **429**, 57–62.
14. H. Goudarzi and P. E. Keivanidis, *ACS Appl. Mater. Interfaces*, 2017, **9**, 845–857.
15. J. Zimmermann, R. Mulet, G. D. Scholes, T. Wellens and A. Buchleitner, *J. Chem. Phys.*, 2014, **141**, 184104.
16. T. C. Wu, D. N. Congreve and M. A. Baldo, *Appl. Phys. Lett.*, 2015, **107**, 031103.
17. B. Y. Lin, C. J. Easley, C. H. Chen, P. C. Tseng, M. Z. Lee, P. H. Sher, J. K. Wang, T. L. Chiu, C. F. Lin, C. J. Bardeen and J. H. Lee, *ACS Appl. Mater. Interfaces*, 2017, **9**, 10963–10970.
18. Y. H. L. Lin, M. Koch, A. N. Brigeman, D. M. E. Freeman, L. Zhao, H. Bronstein, N. C. Giebink, G. D. Scholes and B. P. Rand, *Energy Environ. Sci.*, 2017, **10**, 1465–1475.
19. K.-H. Kim, C.-K. Moon, J. W. Sun, B. Sim and J.-J. Kim, *Adv. Opt. Mater.*, 2015, **3**, 895–899.
20. J. Li, H. Nomura, H. Miyazaki and C. Adachi, *Chem. Commun.*, 2014, **50**, 6174–6176.
21. M. Sarma and K.-T. Wong, *ACS Appl. Mater. Interfaces*, 2018, **10**, 19279–19304.
22. G. Sych, J. Simokaitiene, O. Bezvikonnyi, U. Tsiko, D. Volyniuk, D. Gudeika and J. V. Grazulevicius, *J. Phys. Chem. C*, 2018, **122**, 14827–14837.
23. G. Grybauskaitė-Kaminskiene, K. Ivaniuk, G. Bagdziunas, P. Turyk, P. Stakhira, G. Baryshnikov, D. Volyniuk, V. Cherpak, B. Minaev, Z. Hotra, H. Ågren and J. V. Grazulevicius, *J. Mater. Chem. C*, 2018, **6**, 1543–1550.
24. J. Perez-Prieto, R. E. Galian, M. C. Morant-Minana and M. A. Miranda, *Chem. Commun.*, 2006, 1021–1023.
25. S. Seo, S. Shitagaki, N. Ohsawa, H. Inoue, K. Suzuki, H. Nowatari and S. Yamazaki, *Jpn. J. Appl. Phys.*, 2014, **53**, 042102/042101–042108.
26. P. Y. Chou, H. H. Chou, Y. H. Chen, T. H. Su, C. Y. Liao, H. W. Lin, W. C. Lin, H. Y. Yen, I. C. Chen and C. H. Cheng, *Chem. Commun.*, 2014, **50**, 6869–6871.

27. J. H. Lee, Y. H. Ho, T. C. Lin and C. F. Wu, *J. Electrochem. Soc.*, 2007, **154**, J226-J228.
 28. P. B. Deotare, W. Chang, E. Hontz, D. N. Congreve, L. Shi, P. D. Reusswig, B. Modtland, M. E. Bahlke, C. K. Lee, A. P. Willard, V. Bulovic, T. V. Voorhis and M. A. Baldo, *Nat. Mater.*, 2015, **14**, 1130-1134.
 29. G. J. Kavarnos and N. J. Turro, *Chem. Rev.*, 1986, **86**, 401-449.
 30. M. Koch, G. Licari and E. Vauthey, *J. Phys. Chem. B*, 2015, **119**, 11846-11857.
 31. U. Bhattacharjee, C. Beck, A. Winter, C. Wells and J. W. Petrich, *J. Phys. Chem. B*, 2014, **118**, 8471-8477.
 32. S.-J. He, D.-K. Wang, N. Jiang and Z.-H. Lu, *J. Phys. Chem. C*, 2016, **120**, 21325-21329.
 33. W. B. Davis, W. A. Svec, M. A. Ratner and M. R. Wasielewski, *Nature*, 1998, **396**, 60-63.
 34. H. B. Gray and J. R. Winkler, *Proc. Natl. Acad. Sci.*, 2005, **102**, 3534-3539.
 35. S. Franzen, R. F. Goldstein and S. G. Boxer, *J. Phys. Chem.*, 1993, **97**, 3040-3053.
 36. M. Natali, S. Campagna and F. Scandola, *Chem. Soc. Rev.*, 2014, **43**, 4005-4018.
 37. O. S. Wenger, *Phys. Chem. Chem. Phys.*, 2013, **15**, 10673-10685.
 38. M. Bertocchi, X. F. Zhang, A. Bajpai, J. N. Moorthy and R. G. Weiss, *J. Photochem. Photobiol. A*, 2018, **355**, 467-478.
 39. S. T. Cheung and W. R. Ware, *J. Phys. Chem.*, 1983, **87**, 466-473.
 40. H. Nakanotani, T. Furukawa, K. Morimoto and C. Adachi, *Sci. Adv.*, 2016, **2**, e1501470.
 41. B. Li, L. Gan, X. Cai, X. L. Li, Z. Wang, K. Gao, D. Chen, Y. Cao and S. J. Su, *Adv. Mater. Interfaces*, 2018, **5**, 1800025.
-
1. C.-J. Chiang, A. Kimyonok, M. K. Etherington, G. C. Griffiths, V. Jankus, F. Turksoy and A. P. Monkman, *Adv. Funct. Mater.*, 2013, **23**, 739-746.
 2. N. A. Kukhta, T. Matulaitis, D. Volyniuk, K. Ivaniuk, P. Turyk, P. Stakhira, J. V. Grazulevicius and A. P. Monkman, *J. Phys. Chem. Lett.*, 2017, **8**, 6199-6205.
 3. T. Masuda, Y. Nakano, Y. Takahashi, H. Ito, K. Okinaka, E. Kambe, Y. Kawamura and H. Kuma, *J. Soc. Inf. Disp.*, 2018, **26**, 146-152.
 4. Y. Takita, K. Takeda, N. Hashimoto, S. Nomura, T. Suzuki, H. Nakashima, S. U. S. Seo and S. Yamazaki, *J. Soc. Inf. Disp.*, 2018, **26**, 55-63.
 5. X. Qiao, P. Yuan, D. Ma, T. Ahamad and S. M. Alshehri, *Org. Electron.*, 2017, **46**, 1-6.
 6. C. Xiang, C. Peng, Y. Chen and F. So, *Small*, 2015, **11**, 5439-5443.
 7. M. K. Manna, S. Shokri, G. P. Wiederrecht, D. J. Gosztola and A. J. L. Ayitou, *Chem. Commun.*, 2018, **54**, 5809-5818.
 8. T. N. Singh-Rachford and F. N. Castellano, *Coord. Chem. Rev.*, 2010, **254**, 2560-2573.
 9. N. Yanai and N. Kimizuka, *Chem. Commun.*, 2016, **52**, 5354-5370.
 10. N. Yanai and N. Kimizuka, *Acc. Chem. Res.*, 2017, **50**, 2487-2495.
 11. F. Deng, J. Blumhoff and F. N. Castellano, *J. Phys. Chem. A*, 2013, **117**, 4412-4419.
 12. V. Gray, K. Moth-Poulsen, B. Albinsson and M. Abrahamsson, *Coord. Chem. Rev.*, 2018, **362**, 54-71.
 13. R. Karpicz, S. Puzinas, V. Gulbinas, A. Vakhnin, A. Kadashchuk and B. P. Rand, *Chem. Phys.*, 2014, **429**, 57-62.
 14. H. Goudarzi and P. E. Keivanidis, *ACS Appl. Mater. Interfaces*, 2017, **9**, 845-857.

15. J. Zimmermann, R. Mulet, G. D. Scholes, T. Wellens and A. Buchleitner, *J. Chem. Phys.*, 2014, **141**, 184104.
16. T. C. Wu, D. N. Congreve and M. A. Baldo, *Appl. Phys. Lett.*, 2015, **107**, 031103.
17. B. Y. Lin, C. J. Easley, C. H. Chen, P. C. Tseng, M. Z. Lee, P. H. Sher, J. K. Wang, T. L. Chiu, C. F. Lin, C. J. Bardeen and J. H. Lee, *ACS Appl. Mater. Interfaces*, 2017, **9**, 10963-10970.
18. Y. H. L. Lin, M. Koch, A. N. Brigeman, D. M. E. Freeman, L. Zhao, H. Bronstein, N. C. Giebink, G. D. Scholes and B. P. Rand, *Energy Environ. Sci.*, 2017, **10**, 1465-1475.
19. K.-H. Kim, C.-K. Moon, J. W. Sun, B. Sim and J.-J. Kim, *Adv. Opt. Mater.*, 2015, **3**, 895–899.
20. J. Li, H. Nomura, H. Miyazaki and C. Adachi, *Chem. Commun.*, 2014, **50**, 6174--6176.
21. M. Sarma and K.-T. Wong, *ACS Appl. Mater. Interfaces*, 2018, **10**, 19279–19304.
22. G. Sych, J. Simokaitiene, O. Bezikonny, U. Tsiko, D. Volyniuk, D. Gudeika and J. V. Grazulevicius, *J. Phys. Chem. C*, 2018, **122**, 14827–14837.
23. G. Grybauskaitė-Kaminskiene, K. Ivaniuk, G. Bagdziunas, P. Turyk, P. Stakhira, G. Baryshnikov, D. Volyniuk, V. Cherpak, B. Minaev, Z. Hotra, H. Ågren and J. V. Grazulevicius, *J. Mater. Chem. C*, 2018, **6**, 1543--1550.
24. J. Perez-Prieto, R. E. Galian, M. C. Morant-Minana and M. A. Miranda, *Chem. Commun.*, 2006, 1021–1023.
25. S. Seo, S. Shitagaki, N. Ohsawa, H. Inoue, K. Suzuki, H. Nowatari and S. Yamazaki, *Jpn. J. Appl. Phys.*, 2014, **53**, 042102/042101-042108.
26. P. Y. Chou, H. H. Chou, Y. H. Chen, T. H. Su, C. Y. Liao, H. W. Lin, W. C. Lin, H. Y. Yen, I. C. Chen and C. H. Cheng, *Chem. Commun.*, 2014, **50**, 6869-6871.
27. J. H. Lee, Y. H. Ho, T. C. Lin and C. F. Wu, *J. Electrochem. Soc.*, 2007, **154**, J226-J228.
28. P. B. Deotare, W. Chang, E. Hontz, D. N. Congreve, L. Shi, P. D. Reusswig, B. Modtland, M. E. Bahlke, C. K. Lee, A. P. Willard, V. Bulovic, T. V. Voorhis and M. A. Baldo, *Nat. Mater.*, 2015, **14**, 1130-1134.
29. G. J. Kavarnos and N. J. Turro, *Chem. Rev.*, 1986, **86**, 401-449.
30. M. Koch, G. Licari and E. Vauthey, *J. Phys. Chem. B*, 2015, **119**, 11846–11857.
31. U. Bhattacharjee, C. Beck, A. Winter, C. Wells and J. W. Petrich, *J. Phys. Chem. B*, 2014, **118**, 8471–8477.
32. S.-J. He, D.-K. Wang, N. Jiang and Z.-H. Lu, *J. Phys. Chem. C*, 2016, **120**, 21325–21329.
33. W. B. Davis, W. A. Svec, M. A. Ratner and M. R. Wasielewski, *Nature*, 1998, **396**, 60-63.
34. H. B. Gray and J. R. Winkler, *Proc. Natl. Acad. Sci.*, 2005, **102**, 3534-3539.
35. S. Franzen, R. F. Goldstein and S. G. Boxer, *J. Phys. Chem.*, 1993, **97**, 3040-3053.
36. M. Natali, S. Campagna and F. Scandola, *Chem. Soc. Rev.*, 2014, **43**, 4005--4018.
37. O. S. Wenger, *Phys. Chem. Chem. Phys.*, 2013, **15**, 10673--10685.
38. M. Bertocchi, X. F. Zhang, A. Bajpai, J. N. Moorthy and R. G. Weiss, *J. Photochem. Photobiol. A*, 2018, **355**, 467-478.
39. S. T. Cheung and W. R. Ware, *J. Phys. Chem.*, 1983, **87**, 466-473.
40. H. Nakanotani, T. Furukawa, K. Morimoto and C. Adachi, *Sci. Adv.*, 2016, **2**, e1501470.
41. B. Li, L. Gan, X. Cai, X. L. Li, Z. Wang, K. Gao, D. Chen, Y. Cao and S. J. Su, *Adv. Mater. Interfaces*, 2018, **5**, 1800025.

Table of Contents (TOC) graphic



A triplet-diffusion-singlet-blocking layer and fluorescent dopant enhance blue emission due to triplet-triplet annihilation in an organic light emitting diode structure.